Journal of NUCLEAR SCIENCE and TECHNOLOGY, 32[7], pp. 629~640 (July 1995).

Void Fraction Distribution in BWR Fuel Assembly and Evaluation of Subchannel Code

Akira INOUE,
*Tokyo Institute of Technology**

Tatsuo KUROSU, Toshimasa AOKI, Makoto YAGI,
*Nuclear Power Engineering Corporation***

Toru MITSUTAKE and Shin-ichi MOROOKA
*Nuclear Engineering Lab., Toshiba Corporation****

(*Received January 4, 1994*)

Void fraction measurement tests for BWR fuel assemblies have been conducted as part of a Japanese national project. The aim was to verify the current BWR void fraction prediction method. Void fraction was measured using an X-ray CT scanner. This paper describes typical results of void fraction distribution measurements and compares subchannel-averaged void fraction data with current subchannel analysis codes. The subchannel analysis codes COBRA/BWR and THERMIT-2 were used in this comparison. The agreement between data for an actual BWR fuel assembly with two unheated rods was good, but in the case of many unheated rods, the codes were unable to predict well large void fraction gradient in the radial direction observed in the measured data over the unheated rod region. The prediction errors of COBRA/BWR and THERMIT-2 for the subchannel-averaged void fraction were $\langle A \rangle$ (average of difference between measurement and calculation)$=-1.1\%$, σ (standard deviation)$=5.3\%$ and $\langle A \rangle=-2.2\%$, $\sigma=6.3\%$, respectively.

***KEYWORDS:* BWR type reactors, fuel assemblies, void fraction, X-ray CT scanner, subchannel analysis code, two-phase flow, experimental data, comparative analysis, accuracy**

I. INTRODUCTION

The Ministry of International Trade and Industry (MITI) is sponsoring a national project consisting of various tests to prove LWR (Light Water Nuclear Reactor) reliability as a national project[1]. As a part of this project, the Nuclear Power Engineering Corporation (NUPEC) has carried out "Void Fraction Measurement Test in BWR Fuel Assembly" under the auspices of MITI[2].

In a boiling water nuclear reactor (BWR), void fraction in the coolant flow affects nuclear reactivity and thermal-hydraulic characteristics of the reactor by altering reactor power, coolant flow, pressure, and temperature. Thus, void fraction is one of the most significant variables from the viewpoint of core-fuel design and reactor safety. In addition, when developing new LWR fuel assemblies, thermal-hydraulic tests are at present carried out in out-of-pile test facilities using many full-scale simulated rod assemblies. This type of testing makes the development of a new fuel assembly expensive and time-consuming. Meanwhile, many researchers have put a great deal of effort into developing subchannel analysis codes. However, no subchannel code has yet been proven to offer adequate performance since available subchannel data are limited.

Void fraction measurements in a simulated fuel assembly have been performed by

* *Oh-okayama, Meguro-ku, Tokyo 152.*
** *Toranomon, Minato-ku, Tokyo 105.*
*** *Shinsugita, Isogo-ku, Yokohama 235.*

Nylund[3] in experiments with 36 heater rods arranged in three concentric circular layers surrounding an unheated rod. However, this test section did not simulate a BWR fuel assembly. One of the present authors[4] measured void fraction distributions in a vertical square (4×4) rod array, simulating a BWR fuel assembly, using an X-ray CT scanner system. However, the test pressure (1 MPa) was lower than the actual BWR rated pressure (7 MPa). No void fraction data using a full-scale BWR fuel assembly under BWR conditions has been reported.

The void fraction distribution in a multi-rod assembly with a typical reactor power profile has now been measured by the X-ray CT scanner method to demonstrate the reliability of BWR thermal-hydraulic core design and current subchannel analysis codes. The tests were carried out in an out-of-pile test facility able to simulate the high-pressure, high-temperature fluid conditions found in a BWR. An electrically-heated rod assembly simulates the BWR fuel assembly at full scale.

The primary purposes of this study were to clarify the void fraction distribution in a BWR fuel assembly under steady-state conditions and evaluate the capabilities of current subchannel analysis codes. Regarding the latter purpose, there are two kinds of fluid-field descriptions generally used in two-phase flow analysis, the single- and the two-fluid field model. In this context, it is preferable to compare both kinds of subchannel analysis code with measurements. The single-fluid field subchannel analysis code COBRA/BWR[5] has been used previously in a critical power test[1], and the two-fluid field code THERMIT-2[6], which is generally applied to two-phase flow calculations, was also used.

This paper describes typical results of void fraction distribution as measured by the X-ray CT scanner and compares the subchannel void fraction data with the two subchannel codes.

II. Test Facility and Method

1. Test Loop

Figure 1 is a diagram of the test facility, which is made of SUS304. Demineralized water is used as the cooling fluid. The maximum operating conditions for this loop are 10.3 MPa in pressure, 315°C in temperature, 12 MW in test power, and 33 kg/s in flow rate. Water is circulated by the circulation pump ①, and the coolant flow rate is controlled by the three valves ③ of different sizes. The inlet fluid temperature for the test section ⑤ is controlled by a direct-heating tubular preheater ④. Subcooled coolant flows upward into the test section ⑤, where it is heated and becomes a two-phase flow through the test assembly. The steam, which is separated from the steam-water mixture in the separator ⑦, is condensed using a spray of subcooled water in the steam drum ⑧. The condensed water is then returned to the circulation pump ①. The system pressure in both steady and unsteady state tests is controlled by spray lines ⑨, which have four different-sized valves. The pressurizer ⑥ controls the system pressure when the test assembly power is low. The spray pump ⑩ forces a spray into the steam-drum after the water is cooled with two air-cooled heat-exchangers ⑪.

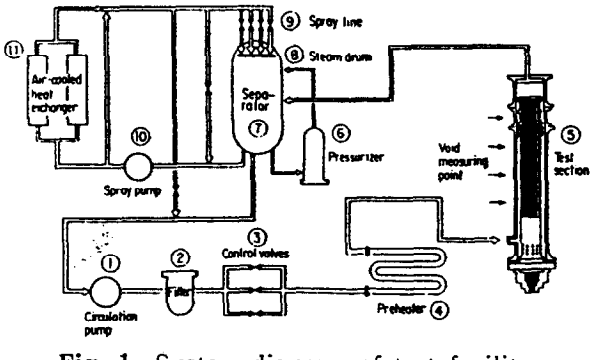

Fig. 1 System diagram of test facility

The test loop has a full range of steady-state void fraction testing capabilities over BWR operating conditions and can also simulate unsteady characteristics, flow changes, power changes and complicated BWR operational transients.

2. Test Section

The test section, shown in **Fig. 2**(a), consists of a pressure vessel, a simulated flow channel, and electrodes. The full-scale BWR simulated fuel assembly is installed within this section.

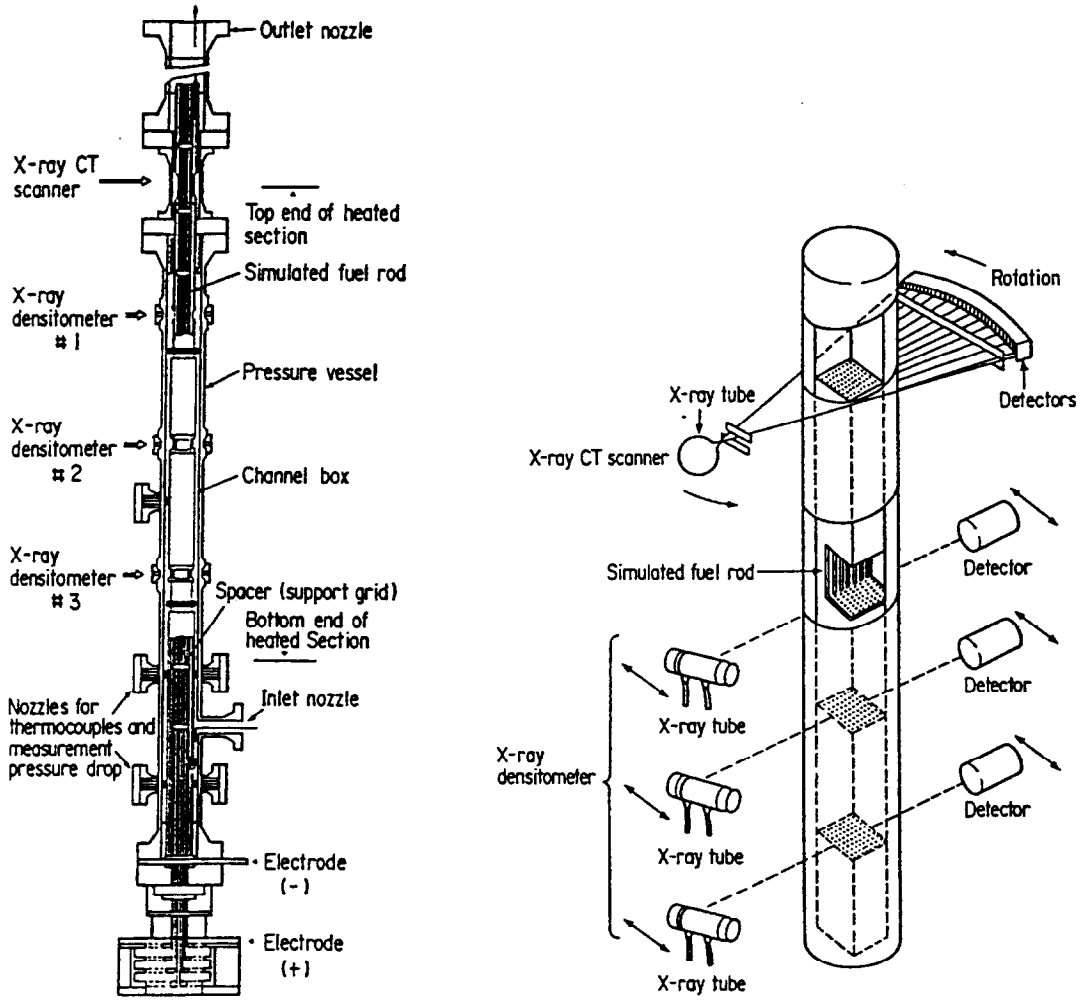

(a) Cross-sectional view of test section (b) Void fraction measurement system

Fig. 2 Test section

The test assembly consists of electrically heated rods. The heater rods are fixed in an array identical to that of the BWR fuel assembly being simulated. Each simulated rod in the test assembly is indirectly heated, as shown in Fig. 4, to simulate an actual reactor power profile generated by nuclear fission.

Three test assemblies were used to measure the effects of radial power distribution on the void fraction distribution. To obtain clearer information, the number of unheated rods was varied among these test assemblies. The radial arrangements of heated and unheated rods are shown in **Fig. 3**; all have a uniform axial heat flux. Test assembly No. 0-1 simulates a current BWR fuel assembly and has two unheated rods. Test assemblies No. 0-2 and No. 0-3 have four and nine unheated rods, respectively.

Figure 4 shows the cross-sectional view of a heated rod. It is of grounded type. The cladding, insulator, and heater are made of inconel, boron nitride, and nichrome, respectively. The heated rod surface temperature is measured by 0.5 mm-diameter chromel-alumel thermocouples. Individual thermocouples are embedded in the cladding surface. Axially, they are positioned mainly at positions just upstream of the spacers. Each heated rod is joined to an X-ray transmission section, which has the same diameter as the heated rod and is made of beryllium (Be).

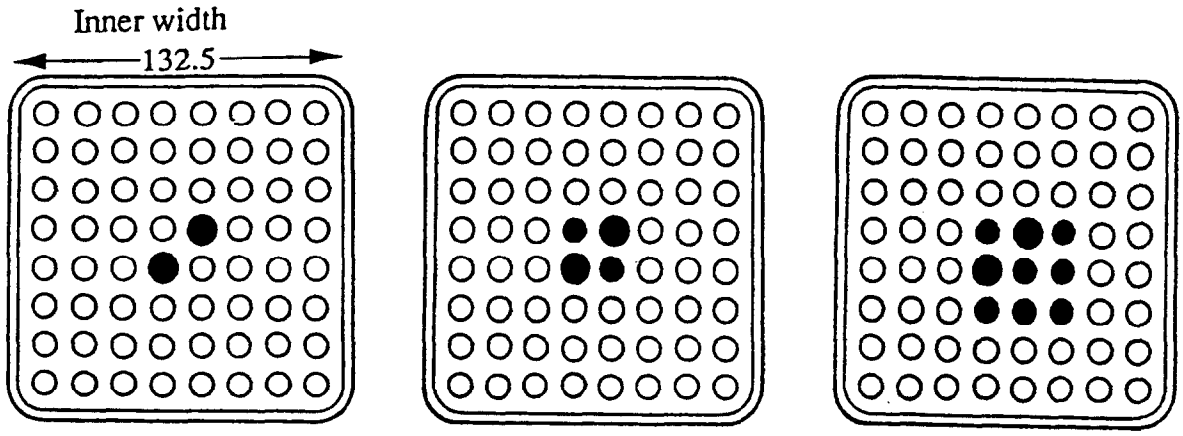

(a) Test assembly 0-1 (b) Test assembly 0-2 (c) Test assembly 0-3

○: Heated rod, ●: Unheated rod
Heated rod diameter: D=12.3 mm, Unheated rod diameter: D=15.0 mm, Rod pitch: s=16.2 mm

Fig. 3 Radial power distribution

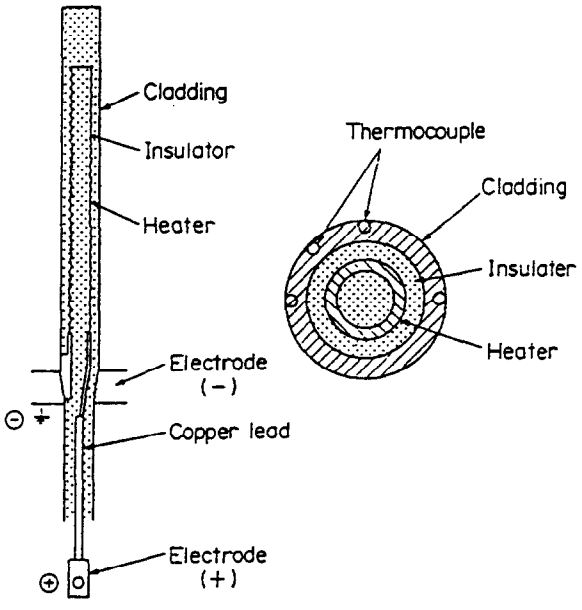

Fig. 4 Cross-sectional view of heated rod

III. Void Measuring System and Other Instrumentation

1. Void Measuring System

This part of the test section has two kinds of void fraction measuring systems, the X-ray CT scanner and the X-ray densitometer shown in Fig. 2(b). **Figure 5** shows the void fraction measuring section, in which the void fraction is measured using an X-ray CT scanner. The X-ray path through the channel wall and rod is made of Be, and the pressure vessel is made of titanium (Ti), to minimize X-ray attenuation in the structure. The X-ray CT scanner measures the void fraction distribution at a point

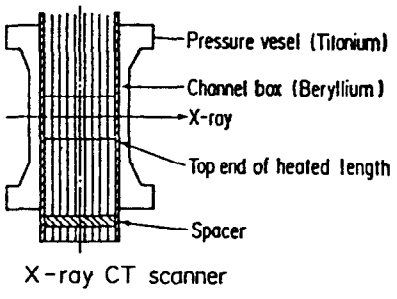

Fig. 5 Void fraction measuring section

4 cm above the heated length. The X-ray densitometer measures void fraction changes during fast transients which the X-ray CT scanner cannot do. **Table 1** shows the basic specifications of the X-ray CT scanner. This CT scanner consists of an X-ray tube and 512 detectors. The X-ray beam is scanned over an object. An outline of the CT scanner principle is shown in **Fig. 6**. As it scans, a fan-shaped X-ray beam is attenuated by the object and the attenuated beam is picked up

Table 1 Specifications of X-ray CT scanner

• Scan method	360° rotation with pulse X-rays
• Type of X-ray beam	Fan-shaped X-ray beam of 34° radiation angle
• Voltage of X-ray tube	Max. 120 kV
• Current	Max. 400 mA
• Scanning time	15 s
• Scanning region	ϕ 300 mm
• Dimensions of reconstruction element	0.3 mm×0.3 mm

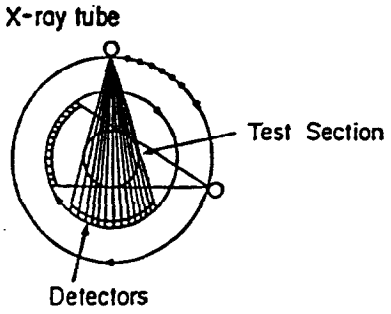

Fig. 6 Scanning method

by the detectors. The X-ray intensity data recorded by the detectors is called the projection data. Complete projection data are obtained for a 360° angle around the object. To avoid the effect of two-phase flow fluctuations on the projection data, a time-averaging technique is used. This means that measurements of a projection data set are repeated to obtain averaged data[4].

A distribution of the linear attenuation coefficient is obtained by reconstructing the projection data. The reconstruction technique is called a filtered back-projection, and has been widely used in the field of nuclear medicine.

All void fraction signals from the detectors are calibrated by the signal from a reference detector to improve the signal-to-noise ratio.

Before actual void fraction measurements, position coordinates are calibrated at room temperature with the test section empty. They are then repeated with the section filled with water and at operating temperature with non-boiling water. Frequent measurements through a standard absorber are made to permit the correction of electronic drift.

2. Other Instrumentation

Diaphragm transducers are used to measure system pressure and differential pressure along the axis of the test section. The inlet flow rate is measured by a turbine flow meter. Double thermistors are used to measure inlet fluid temperature.

Table 2 shows the estimated accuracy of the various measurements. Three kinds of void fraction variables are used: the local void fraction on a 0.3×0.3 square pixel element; the subchannel-averaged void fraction, which is averaged over more than 400 pixel elements; and the cross-sectional averaged void fraction, which is more than 10^5 pixel elements. The accuracy of these void fractions depends on the photon statistics of the X-ray source, the detector non-linearlity and the accuracy of fluid condition (temperature and pressure) measurements.

Table 2 Estimated accuracy

Quantity	Accuracy
Pressure	1%
Flow	1%
Power	1.5%
Inlet fluid temp.	1.5°C
X-ray CT scanner	
Local void fraction	8%
Subchannel void fraction	3%
Cross-sectional void fration	2%

IV. Experimental Method and Test Conditions

Steady-state tests are conducted by controlling a flow rate, inlet fluid temperature, and pressure. When the conditions have stabilized sufficiently, void fraction measurements are begun.

The ranges of experimental conditions are as follows:

Pressure: 1-8.6 MPa
Mass flux: 284-1,988 kg/m²·s
Quality: 0.0-0.25.

V. Results and Discussions

1. Void Fraction Distribution

Photographs 1(a) and (b) show typical local void fraction distributions measured by the X-ray CT scanner. In these figures, the void fraction is represented by a color gradation from blue to red. The axial power distribution is uniform and the radial power distributions for test assemblies No. 0-1, 0-2 and 0-3 are shown in Fig. 3.

Photograph 1(a) shows the effect of quality on the local void fraction distribution for test assembly No. 0-1. Pressure and mass flux are 7.3 MPa and 1,562 kg/m²·s, respectively. These are the rated conditions for a BWR. In the case of quality=1.8% (see Photo. 1(a)-(1)), a void fraction is measured only in the inner subchannels and near the corner

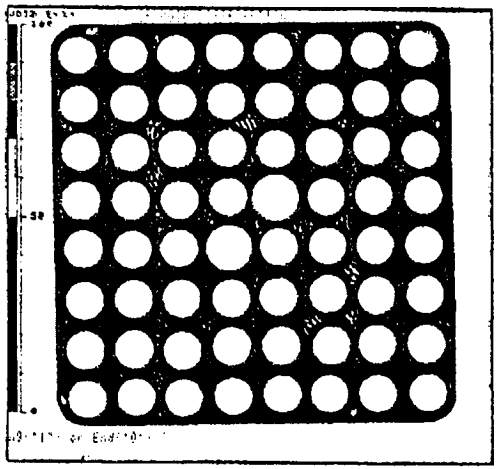

(1) X=1.8%

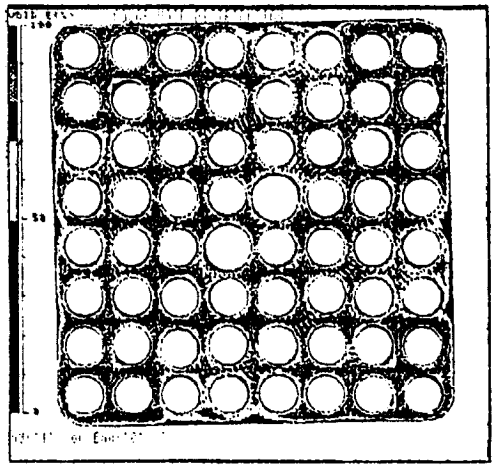

(2) X=12.0%

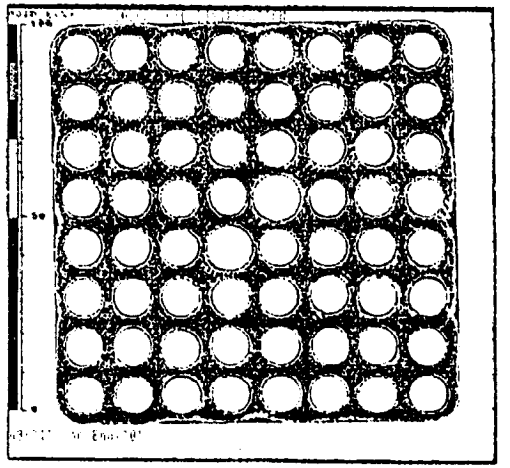

(3) X=17.9%

Pressure: 7.3 MPa, Mass flux: 1,562 kg/m²·s, Test assembly 0-1

(a) Effect of quality

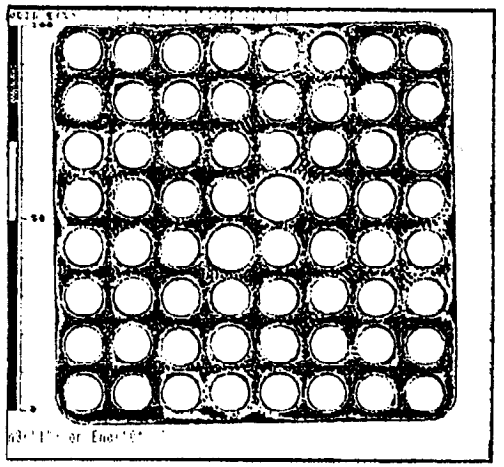

(1) Test assembly 0-1

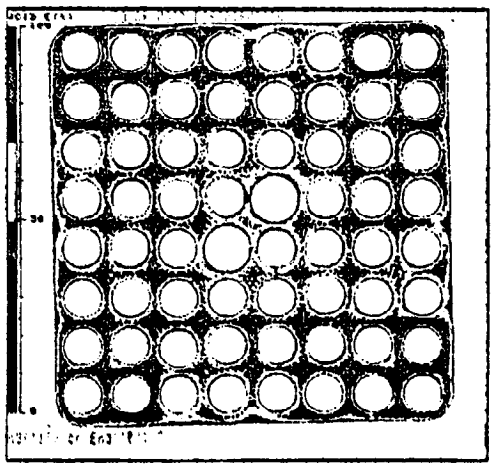

(2) Test assembly 0-2

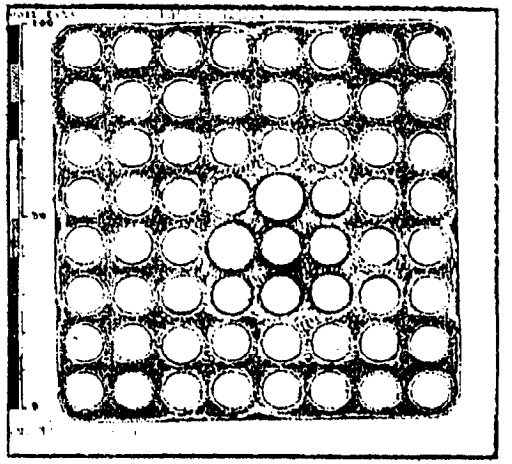

(3) Test assembly 0-3

Pressure: 7.3 MPa, Mass flux: 1,562 kg/m²·s, Quality: 12%

(b) Effect of unheated rods

Photo. 1 Typical local void distribution by X-ray CT scanner

rods. Vapor is present in the subchannels; that is, the flow regime is bubbly. However, when the quality is raised to 12.0% (see Photo. 1(a)-(2)), the void fraction increases over the whole-cross section. A low void fraction region, corresponding to a liquid film, exists on the channel wall and at the rod surfaces; that is the annular flow regime. In the case of quality=17.9% (see Photo. 1 (a)-(3)), the void fraction distribution becomes radially uniform, and a low void fraction region, again corresponding to a liquid film, still exists on the channel wall and at the rod surfaces.

Photograph 1(b) shows the effect of unheated rods on the local void fraction distribution. The void fraction in the center region of which is surrounded by unheated rods, is lower than that on the periphery of the cross section between the channel wall and the second row of the rod array. The void fraction in the region surrounded by unheated rod decreases as the number of unheated rod increases. On the other hand, the void fraction on the periphery inevitably increases, because the rod power fraction in this region increases to maintain a constant assembly power, and the amount of vapor generated on the periphery increases.

2. Cross-Sectional Averaged Void Fraction

Figures 7(a) and (b) show the effect of parameters on the cross-sectional averaged void fraction. Figure 7(a) shows the relationship between cross-sectional averaged void fraction and cross-sectional averaged quality. The void fraction increases sharply as the quality increases up to a quality of about 10%, and then increases more gradually. Figure 7(b) shows that the void fraction increases as the mass flux increases. The influence of mass flux on the void fraction might be understood as follows. As the mass flux increases, both the liquid- and vapor-phase velocities increase. However, the liquid-phase velocity increases faster than the vapor-phase velocity since the resistance to vapor phase flow increases in proportion to the square of the vapor-phase velocity. The result is a decrease in the slip ratio. This kind of mass flux effect is realized also seen in one-dimensional flows such as in a tube.

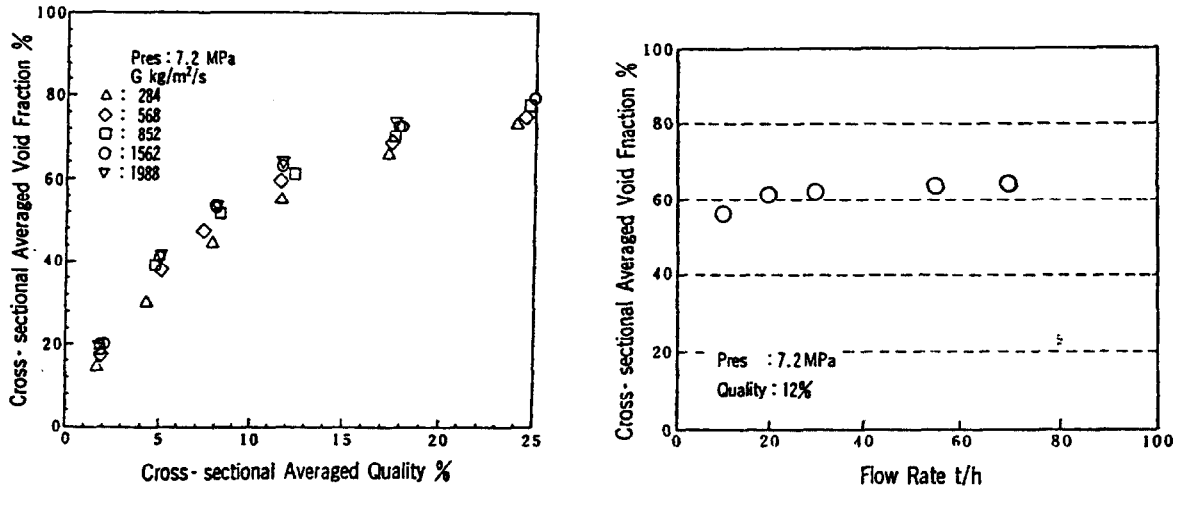

(a) Quality effect (b) Mass flux effect

Fig. 7 Quality effect and mass flux effect on cross-sectional averaged void

Figure 8 shows the effect of the number of unheated rods on the cross-sectional averaged void fraction. It is clear that the number of unheated rods has a negligible effect on the void fraction.

3. Evaluation of Subchannel Analysis Codes

The subchannel analysis codes COBRA/BWR[5] and THERMIT-2[6] were used in this study.

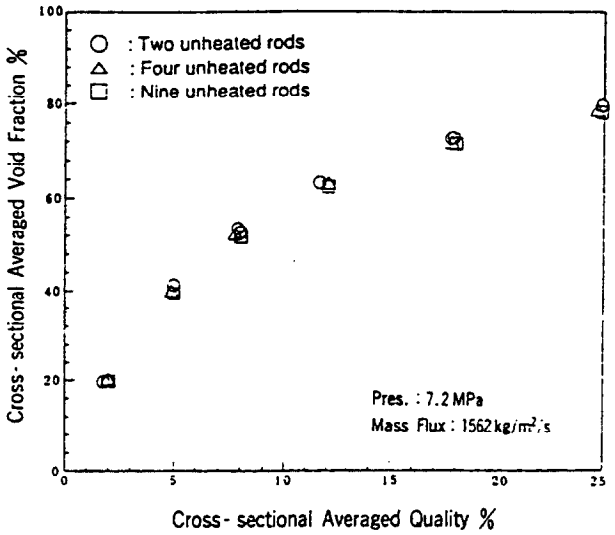

Fig. 8 Effect of unheated rod on cross-sectional averaged void fraction

COBRA/BWR is a modified version of COBRA-4[7] for BWR two-phase flow applications. The basic equations of mass, energy, and momentum are derived for each subchannel. These equations are shown in **Table 3.** The code is based on a mixture flow model called the single-fluid field model, and treats the two-phase flow behavior as a single-fluid flow while taking account of the difference between the liquid- and vapor-phase velocities. It also takes account of two-phase flow mixing and the void drift model, which follows the Lahey formulation as shown in **Table 4.** Of the constitutive equations given in Table 4, the void drift model is developed to describe a peculiar characteristic of spatial two-phase

Table 3 Fundamental equations

(1) Two-phase mix flow—three equations (COBRA/BWR)

Mass: $A\frac{\partial \rho}{\partial t}+\frac{\partial m}{\partial z}+[DC]^T W=0$

Energy: $A\frac{\partial(\rho h)}{\partial t}+\frac{\partial(mh)}{\partial z}+[DC]^T h^* W=q'$

Momentum: $\frac{\partial m}{\partial t}+\frac{\partial(mu)}{\partial z}+[DC]^T u^* W+A\frac{\partial p}{\partial z}=F$

Lateral momentum: $\frac{\partial W}{\partial t}+\frac{\partial(u^* W)}{\partial z}+\frac{\partial(vW)}{\partial x}-[DC]P=C$

(2) Two-phase separated flow—six equations (THERMIT-2)
(subscript $k=g$: gas, l: liquid)

Mass: $\frac{\partial}{\partial t}(\alpha_k \rho_k)+\nabla(\alpha_k \rho_k V_k)=\Gamma_k$

Energy: $\frac{\partial}{\partial t}(\alpha_k \rho_k h_k)+\nabla(\alpha_k \rho_k h_k V_k)=P\nabla(\alpha_k V_k)-p\frac{\partial}{\partial t}(\alpha_k)+\Gamma_k h_k+Q_i$

Momentum (x, y, z): $\frac{\partial}{\partial t}(\alpha_k \rho_k V_k)+\alpha_k \rho_k V_k \nabla(V_k)=-\alpha_k \nabla P+\alpha_k \rho_k g-F_i$

Table 4 Two-phase flow correlations

	THERMIT-2	COBRA/BWR
Interfacial shear	$F_i=\frac{4\sqrt{\alpha}}{D}C_d\frac{\rho_v \lvert V_l \rvert V_r}{2}$	(Void fraction correlation: Drift flux model)
Wall friction	Blasius model aRe_l^{-b}	aRe^{-b}
Two-phase multiplier	Martinelli-Nelson multiplier	Martinelli-Nelson multiplier
Subcooled boiling	Ahmad model	Levy model subcool boiling initiation liquid phase enthalpy profile-fit
Crossflow loss K_{cros}	aRe_l^{-b}	Constant
Mixing	Two-fluid void drift Lahey model	Void drift Lahey model
	$(\langle\alpha\rangle_i-\langle\alpha\rangle_j)_{FD}=K_M\frac{\bar{\alpha}}{\bar{G}}(G_i-G_j)$	$(\langle\alpha\rangle_i-\langle\alpha\rangle_j)_{FD}=\frac{\bar{\alpha}}{\bar{G}}(G_i-G_j)$

FD: Fully developed, K_M: Constant

flow distributions: lower coolant mass flux subchannels have lower qualities.

THERMIT-2 is based on a separated flow model called the two-fluid field model. The basic equations and constitutive equations are shown in Tables 3 and 4. This code has two mass, two energy, and six momentum conservation equations in a three-dimensional formulation. The constitutive equations are formulated for each fluid. This two-fluid field model has the advantage of flexibility in treating non-equilibrium two-phase flows.

In this subchannel analysis, the rod assembly is radially divided into subchannels as shown in **Fig. 9**. There are 45 subchannels for a half assembly model, assuming diagonal symmetry, with 24 axial nodes.

In this study, the number of unheated rods near the center of the assembly is varied as shown in Fig. 3. The rod assembly is divided into five zones, as shown in **Fig. 10**, to clarify the radial void fraction distribution more easily. These subchannel analysis codes are evaluated using the zone-averaged and subchannel-averaged void fraction data.

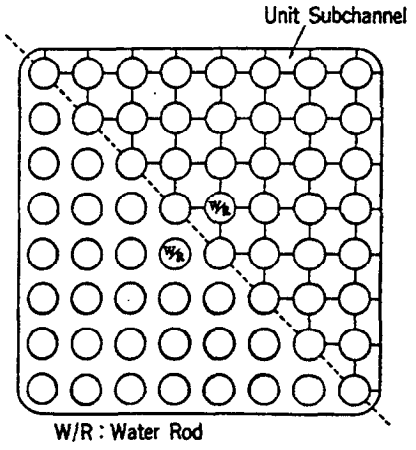

Fig. 9 Subchannel division

Figure 11 (1) compares the test data with the results calculated by the COBRA/BWR code for test assembly No. 0-1. The pressure and mass flux conditions are BWR normal operating conditions. The results indicate a weak convex distribution in the radial direction with a maximum at INR2, the half distance between the channel wall and the center of the cross section. This tendency is clearly

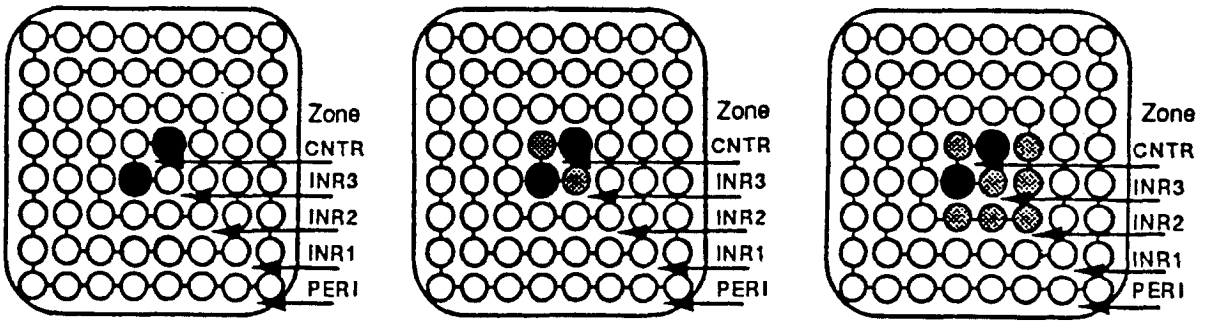

(1) Test assembly 0-1 Two unheated rods (2) Test aseembly 0-2 Four unheated rods (3) Test assembly 0-3 Nine unheated rods

Fig. 10 Five zone name and unheated rod arrangement

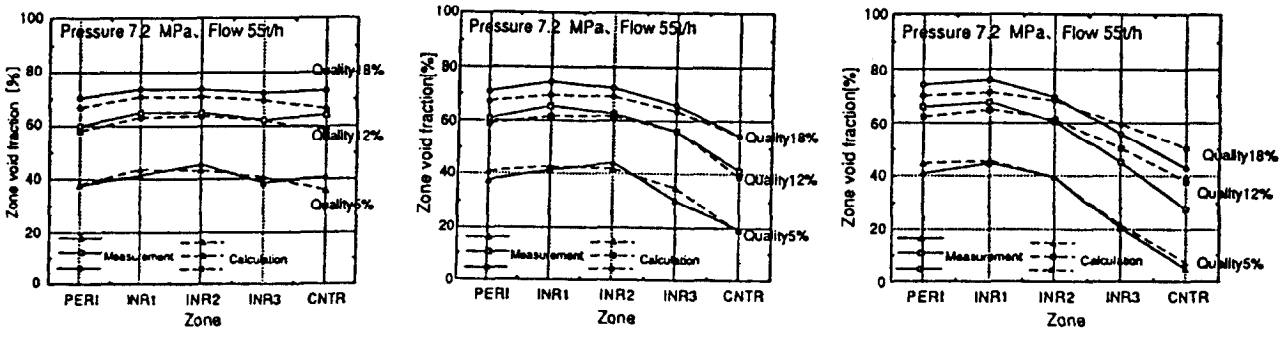

(1) Two unheated rods (2) Four unheated rods (3) Nine unheated rods

Fig. 11 Radial void fraction distribution comparison of COBRA/BWR code

observed even in the lowest quality case of 5%. The radial void fraction distribution becomes flatter as the quality increases. A comparison with the test data shows that this code predicts the radial void fraction distribution well on the whole, except at INR3 and CNTR. The measured void fraction at CNTR is larger than that at INR3. On the other hand, the calculated void fraction at CNTR is smaller than that at INR3. This same result is also predicted by THERMIT-2, as shown in Fig. 12(1). The power density at CNTR is smaller than that at INR3. It seems, therefore, that the void fraction at CNTR should be smaller than that at INR3 because vapor generation at CNTR is less than at INR3. However, the measured results are contrary to the calculations. The reason for this is not clear, but the measurements suggest that the vapor phase enters CNTR from INR3, the neighboring region. The void drift model could be responsible for this kind of vapor-phase transport in a certain direction, while a pressure-differential induced flow, a diversion cross flow, would not cause a larger void fraction at CNTR than at INR3, which is upstream side of CNTR. However, it is difficult to gain a clear understanding without additional information, such as the mass flux, quality, and cross flow distributions.

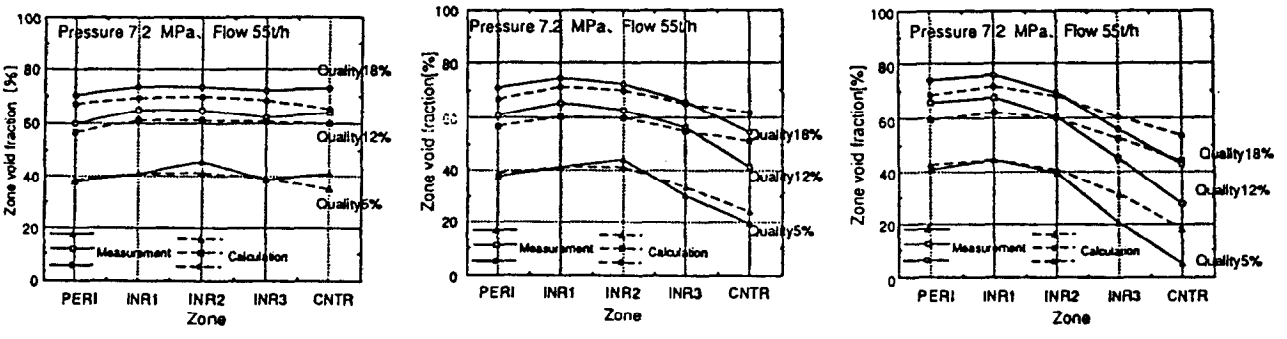

(1) Two unheated rods (2) Four unheated rods (3) Nine unheated rods

Fig. 12 Radial void fraction distribution comparison of THERMIT-2 code

Figures 11(2) and (3) show measured radial void fraction distributions for test assemblies No. 0-2 and 0-3 with four and nine unheated rods, respectively, as well as the results calculated by COBRA/BWR. Also, Fig. 12(2) and (3) compares the test data with THERMIT-2. The thermal-hydraulic conditions in Fig. 11 are the same as in Fig. 12. The measured void fraction at INR3 and CNTR decreases as the number of unheated rods increases. In particular, when there are nine unheated rods (test assembly No. 0-3, Figs. 11(3) and 12(3)), the void fraction gradient is very large across the boundary of the unheated rod region and the void fraction at INR2 is 20% larger than at INR3 in the case of quality =5%. Both codes predict well the effects of unheated rods on the void fraction distribution. The predictive capability of COBRA/BWR is slightly better than that of THERMIT-2. The reason for this is that COBRA/BWR does not consider void drift transport among inner subchannels and THERMIT-2 does. Void drift transport causes a void fraction increase in regions with a low coolant power density per unit coolant flow rate, though it resulted in an overprediction in the cases of four and nine unheated rods as seen in Figs. 12(2) and (3). The mechanism for this result is explained as follows. A lower coolant power density, generally speaking, produces a higher mass flux in a certain subchannel. Considering the void drift phenomena, the vapor phase moves from a region of lower mass flux to one of higher mass flux. This causes a void fraction increase in the higher mass flux region as compared with the void fraction expected from the generated vapor mass flux. Thus, the void fraction calculated by THERMIT-2 were larger at INR3 and CNTR than those by COBRA/BWR. If this kind of modifica-

tions could be made to THERMIT-2, the overprediction in the case of the four and nine unheated rods could be reduced.

We found that the calculated void fraction deviated from the measurements, even at a quality of 5%. As Figs. 11(3) and 12(3) show, both codes fail to predict large void fraction gradients, and the maximum gradient of 20% occurs near INR2 and CNTR in the case of the nine unheated rods.

Figures 13 and **14** compares all the subchannel data. The following quantity is defined to examine the accuracy of these codes:

$$A=(\text{calculated value})-(\text{measured value})$$

The prediction error of COBRA/BWR and THERMIT-2 for the subchannel void fraction is $\langle A\rangle=-1.1\%$, $\sigma=5.3\%$ and $\langle A\rangle=-2.2\%$, $\sigma=6.3\%$, respectively, where $\langle . \rangle$ denotes the average of the value and σ the standard deviation.

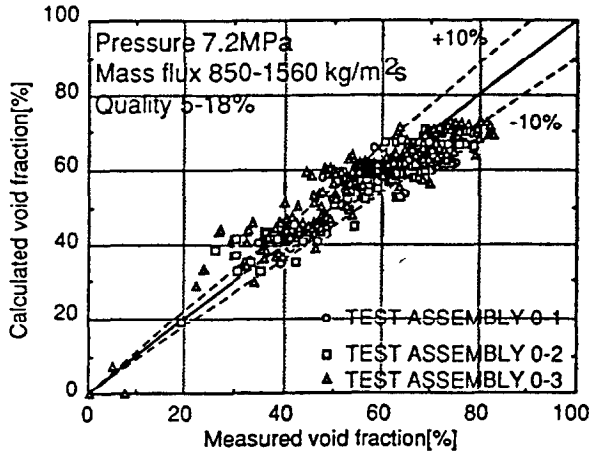

Fig. 13 Subchannel void fraction comparison of COBRA/BWR for test assembly 0-1, 0-2, 0-3

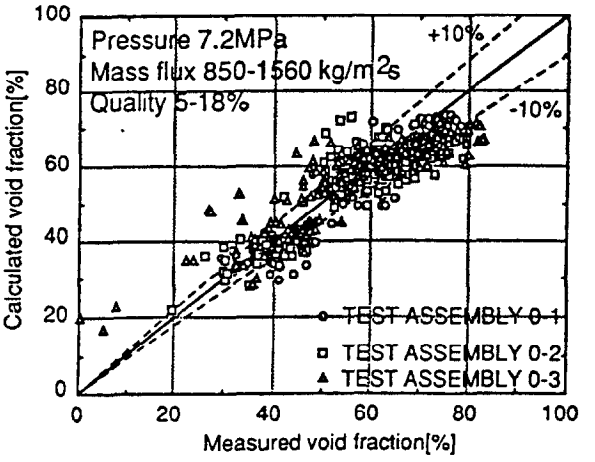

Fig. 14 Subchannel void fraction comparison of THERMIT-2 for test assembly 0-1, 0-2, 0-3

Given these prediction errors, it can be said that the subchannel analysis codes are suitable for the prediction of two-phase flow distributions within BWR rod assemblies. However, to fully clarify the void drift mechanism acting within rod assemblies, it will be necessary to obtain more detailed information about the two-phase flow distribution, such as the mass flux, quality, and cross flows.

VI. Conclusion

Void fraction measurements for a full-scale BWR rod assembly have been conducted under BWR two-phase flow conditions using an X-ray CT scanner. The major conclusions of this work are as follows:

(1) The local void fraction distribution in a BWR fuel assembly under BWR conditions was measured using the X-ray CT scanner.

(2) Unheated rods have a negligible effect on the cross-sectional averaged void fraction.

(3) The radial void fraction distribution was measured with various numbers of unheated rods. The unheated rods cause a large void fraction gradient across the boundary of the region including the unheated rods.

(4) The subchannel analysis codes COBRA/BWR and THERMIT-2 were compared with the subchannel-averaged void fraction data. Agreement with data for an actual BWR fuel assembly with two unheated rods was good, but in the case of many unheated rods, the codes were unable to predict the large measured void fraction gradient well.

(5) The overall prediction errors of COBRA/BWR and THERMIT-2 for the subchannel void fraction were about 6% at most. This means that these subchannel analysis codes are well suitable for the prediction of two-phase flow distributions within BWR rod assemblies.

[NOMENCLATURE]

g: Gravitational constant
h: Enthalpy
m: Axial mass flow rate
q': Heat input
u: Axial two-phase flow velocity
v: Lateral two-phase flow velocity
A: Subchannel flow area
C: Lateral frictional loss
F: Axial frictional loss
i: Interfacial friction
P: Pressure
Q_i: Heat input
W: Lateral mass flow rate
X: Lateral distance
Z: Axial distance
g: Mass generated quantity
ρ: Two-phase flow density
σ: Standard deviation
[DC]: Difference operator
(Subscripts)
g: Vapor
l: Liquid
R: Relative value
(Superscripts)
*: Convective variable

ACKNOWLEDGMENTS

The authors are grateful to The Ministry of International Trade and Industry for permission to publish this paper.

—REFERENCES—

(1) YOSHIDA, H., AKIYAMA, M., INOUE, A.: Proving test of thermal-hydraulic design basis reliability of BWR fuel assembly, *Proc. 2nd Int. Topical Meeting on Nucl. Power Plant Thermal-Hydraulics and Operations*, Vol. 4, 20-27 (1986).
(2) MOROOKA, S., INOUE, A., OISHI, M., AOKI, T., NAGAOKA, K., YOSHIDA, H.: In-bundle void fraction measurement of BWR fuel assembly by X-ray CT scanner, *ICONE-1*, a-38, 237-243 (1991).
(3) NYLUND, O.: Full-scale loop studies of BHWR and BWR fuel assemblies, *Asea Res.*, 10, 63 (1969).
(4) MOROOKA, S., ISHIZUKA, T., IIZUKA, M., YOSHIMURA, K.: Experimental study on void fraction in a simulated BWR fuel assembly (Evaluation of cross-sectional averaged void fraction), *Nucl. Eng. Des.*, 114, 91-98 (1989).
(5) MITSUTAKE, T., TERASAKA, H., YOSHIMURA, K., OISHI, M., INOUE, A., AKIYAMA, M.: Subchannel analysis of a critical power test, using simulated BWR 8×8 fuel assembly, *ibid.*, 122, 235-254 (1990).
(6) KELLY, J.E., KAO, S.P., KAZIMI, M.S.: THERMIT-2, a two-fluid model for light water reactor subchannel analysis, *MIT-EL-81-014*, (1981).
(7) STEWART, C.W., WHEELER, C.L., CENA, R.J., MCMONAGLE, C.A., CUTA, J.M., TRENT, D.S.: COBRA-IV: The model and the method, *BNWL-2214*, (1977).